A New Inverse Modeling Approach for Emission Sources based on the DDM-3D and 3DVAR techniques: an application to air quality forecasts in the Beijing–Tianjin–Hebei Region

Xinghong Cheng[1], Zilong Hao[2], Zengliang Zang[2], Zhiquan Liu[3], Xiangde Xu[1], Shuisheng Wang[4], Yuelin Liu[5], Yiwen Hu[6], Xiaodan Ma[6]

1. State Key Lab of Severe Weather & Key Laboratory for Atmospheric Chemistry, Chinese Academy of Meteorological Sciences, Beijing 100081, China

2. Institute of Meteorology and Oceanography, National University of Defense Technology, Nanjing 211101, China

3. National Center for Atmospheric Research, Boulder, CO, USA

4. GZ Source Clear Tech. Co., Ltd., Guangzhou 510630, China

5. College of Architecture and Environment, Sichuan University, Chengdu 610065, China

6. Nanjing University of Information Science and Technology, Nanjing 210044, China

Correspondence to: Xinghong Cheng (cxingh@cma.gov.cn) and Zengliang Zang (zzlqxxy@163.com)

Abstract. We develop a new inversion method which is suitable for linear and nonlinear emission sources (ES) modeling, based on the three-dimensional decoupled direct (DDM-3D) sensitivity analysis module in the Community Multiscale Air Quality (CMAQ) model and the three-dimensional variational (3DVAR) data assimilation technique. We established the explicit observation operator matrix between the ES and receptor concentrations, and the background error covariance (BEC) matrix of the ES which can reflect the impacts of uncertainties of the ES on assimilation. Then we constructed the inversion model of the ES by combining the sensitivity analysis with 3DVAR techniques. We performed the simulation experiment using the inversion model for a heavy haze case study in the Beijing-Tianjin-Hebei (BTH) region during December 27-30, 2016. Results show that the spatial distribution of sensitivities of SO_2 and NO_X ES to their concentrations, as well as the BEC matrix of ES, are reasonable. Using a *posteriori* inversed ES, underestimations of SO_2 and NO_2 during the heavy haze period are remarkably improved, especially for NO_2. Spatial distributions of SO_2 and NO_2 concentrations simulated by the constrained ES were more accurate compared with a *priori* ES in the BTH region. The temporal variations in regionally averaged SO_2, NO_2, and O_3 modelled concentrations

using a *posteriori* inversed ES are consistent with in-situ observations at 45 stations over the BTH region, and simulation errors decrease significantly. These results are of great significance for: studies on the formation mechanism of heavy haze; reducing uncertainties of ES and its dynamic updating; providing accurate 'virtual' emission inventories for air-quality forecasts and decision-making services for optimization control of air pollution.

1. Introduction

Since the implementation of the Air Pollution Prevention and Control Action Plan in September 2013, urban air quality in China has improved overall. However, heavy haze frequently occurs over Beijing-Tianjin-Hebei (BTH) and the surrounding region in winter. In recent years, many researchers have studied the formation mechanism of heavy haze in the BTH region (Huang et al., 2014; Cheng et al., 2016; Liu et al., 2016). These studies have shown that rapid conversion from primary gas pollutants to particulates is an internal triggering factor for the "explosive" and "persistent" heavy haze (Wang et al., 2014), and secondary particulate concentrations, such as sulfate and nitrate, account for a significant percentage of $PM_{2.5}$. Thus, effectively controlling the emissions of precursors of secondary aerosols (such as SO_2 and NO_x) is important for reducing environmental, economic, and human health problems caused by $PM_{2.5}$ concentrations (Huang et al., 2014).

Emission inventories provide important fundamental data for investigating the causes of air pollution, and atmospheric chemical transport model (ACTM). Uncertainties in ES are a major factor in determining the simulated and forecast accuracy of the ACTM, and these uncertainties can greatly affect the design of ES control strategies (Tang, 2006). The methods for establishing an emission inventory include the bottom-up approach based on human activities, energy consumption statistics, and various emission factors, as well as top-down inversion modeling of ES based on monitoring data of air pollutants using satellite remote sensing and ground observations. Many studies have established various ES inventories in China using the bottom-up approach, e.g., Bai et al., 1996; Streets et al., 2003; Zhang et al., 2009, 2012; Cao et al., 2011; Zhao et al., 2012; Zhao et al., 2015; and Li et al., 2017. However, the ES estimated by this method differ greatly due to large uncertainties in the statistical data, emission factors, and spatiotemporal apportionment coefficients (Ma et al., 2004). Moreover, real-time updates of emission inventories are difficult to achieve because of its rapid spatiotemporal variations

due to high-speed urbanization, and a delay in the release of statistical data of approximately 1–2 years. The top-down approach is a useful supplement to bottom-up estimates, which are subject to uncertainties in emissions factors and activities (Streets et al., 2003). Inverse modeling, in which emissions are optimized to reduce the differences between simulated and observed data, is a powerful method that eliminates the problems of the bottom-up approach.

Over the past decade, many researchers have tried to find an ideal inversion modeling tool that improve the spatiotemporal distribution of ES. With the development of data assimilation technology and ACTM, constraining the strength of ES using ACTM has become one of the main top-down inversion methods (Enting, 2002; Sportisse, 2007). Researchers have primarily constrained the ES of weak active chemical pollutants, such as NO_x, CO, CO_2, SO_2, CH_4, and CHOCHO using the following methods: mass balance (Martin et al., 2003; Wang et al., 2007; Yang et al., 2011), back-trajectory inverse modeling (Manning et al., 2011), adjoint modeling (Liu et al., 2005; Koohkan et al., 2013; Zhang et al., 2016; Wang et al., 2018), Bayes estimation theory (Kopacz et al., 2009), ensemble Kalman-filtering (EnKF, Zhu et al., 2006, 2018; Barbu et al., 2009; Tang et al., 2011, 2016; Miyazaki et al., 2012; Mijling et al., 2012; Wang et al., 2016; Peng et al., 2017; Chen et al., 2019; Dai et al., 2021), the four-dimension variational (4DVAR) technique (Elbern et al., 2000, 2007; Gilliland et al., 2006; Napelenok et al., 2008; Henze et al., 2009; Stavrakou et al., 2009; Corazza et al., 2011; Jiang et al., 2011), an adaptive nudging scheme in the CMAQ model (Xu et al., 2008; Cheng et al., 2010), inversion algorithms combining pollutant dispersion models and a Monte Carlo simulation (Yang et al., 2013). Results show that using an inversion modeling approach to retrieve the spatial distribution of ES can greatly improve air quality simulations and forecasts by the ACTM. Many studies have achieved a certain amount of improvement using the EnKF and 4DVAR methods. The advantage of the EnKF method is that the observation operator is implicit in the assimilation process of ES, and it avoids developing the tangent linear and adjoint models. For example, the fully coupled “online”Weather Research and Forecasting model coupled with Chemistry (WRF-Chem) are used as the forward model to relate the SO_2 emissions to the simulated concentration, and efficiently update the emissions based on the routine surface SO_2 observations (Dai et al.,2021).However, this method has stricter requirements for error perturbations in ES and the construction of bias-correction models. In addition,

the large number of ensemble members in the EnKF method leads to a huge computational cost. Some studies adopted the 4DVAR method to inverse the ES of NO_x and CO based on the Goddard Earth Observing System (GEOS)-Chem adjoint model. However, the GEOS-Chem model is often used to simulate large-scale physical and chemical processes and rarely utilized in urban air quality forecasts because its spatial resolution is too coarse. This method also has high computational costs due to the gradient calculation of the objective function.

The 3DVAR method is a generalization of optimal interpolation methods. It has the advantages of conveniently adding dynamical constraints and directly assimilating unconventional observation data (Li et al., 2013). 3DVAR is widely-used in the assimilation of meteorological and atmospheric chemical data due to simplicity, ability to use complex observations operators, and low computational cost. However, this method has two requirements: assimilated variables must remain relatively stationary within the assimilation window, and the method must be coordinated between the assimilated initial field and the iterative integration of the model. To apply the 3DVAR method to inverse ES, it is necessary to construct an inversion model that can satisfy the aforementioned requirements. Firstly, although ES have monthly, seasonal, and annual variations, the variation of ES is constant within a short period (e.g., for an assimilation window of 1 hour). Secondly, the assimilation effect of ES depends on the quality of observation data and the consistency between observed and simulated values. To ensure consistency between observations and simulations, the sensitivity of the receptor's concentrations with respect to the ES should be accurately calculated (Hu et al., 2009). Using the three-dimensional decoupled direct (DDM-3D) sensitivity analysis method within the CMAQ model, reasonable sensitivity coefficients between ES and the receptor's concentrations can be calculated. This coefficient matrix is then used in the 3DVAR assimilation process, which ensures consistency between the ES and the modelled results. Thus, the top-down 3DVAR constraint methods for ES based on the first- or high-order DDM-3D sensitivity analysis techniques can maintain the coordination between assimilated field of ES and simulated concentration of air pollutants.

The primary methods used to calculate the S-R relationship include the brute force, the adjoint, and the DDM-3D method. Many studies have shown that these methods can improve ES inventories constructed by bottom-up methods for NO_x (Napelenok et al., 2008), CO (Bergamaschi et al., 2000 and

Heald et al., 2004), NH3 (Gilliland et al., 2003), and EC (Hu et al., 2009). The adjoint method is a backward-sensitivity calculation method, while brute force and DDM-3D are forward-sensitivity calculation methods. For inverse modeling of pollution sources with single receptor, the backward-sensitivity method is more suitable, with low computation costs for certain grid sizes in a given time period, but it is not suitable for ES with multiple receptors, which result in high computational costs (Hu et al., 2009; Wang et al., 2013). The forward-sensitivity calculation method is more suitable for inversing the ES based on observed data from satellites or multiple surface stations (Hu et al., 2009). Cohan et al. (2002) introduced the DDM-3D method to the CMAQ model, and created the CMAQ-DDM-3D module for low-order sensitivity calculations in early 2010. In 2014, they added a high-order calculation module for particles (High-Order DDM-3D for Particular Matter; HDDM3D/PM) in the newly released version of CMAQ model. Wang et al. (2013) claim that the sensitivity calculation results using the DDM-3D method are more reasonable than the brute force method. Some studies have used the DDM-3D method (Napelenok et al., 2008; Hu et al., 2009) or a combination of the DDM-3D and a discrete Kalman-filter method (Wang et al., 2013) in conjunction with measurements from satellite and ground observations to inverse BC and NO_x ES in the United States. Because inverse modeling of ES based on discrete Kalman-filtering is more suitable for linear systems, we use the DDM-3D method to calculate the S-R linear and non-linear relationship.

The results of inverse modeling are very sensitive to uncertainties in the ES of NOx, NH_4 and inorganic aerosols (Zhang et al., 2016). Impact of uncertainties in the ES on the assimilation effects need to be considered in the top-down inversion model. The top-down 3DVAR inversion methods developed in this study can include the impacts of ES uncertainties by the BEC matrix of ES based on multiple sets of ES. We developed a new inverse modeling approach for ES that combines the DDM-3D sensitivity analysis method with the 3DVAR assimilation technique, and then applied it to a case study during a typical heavy haze episode. This paper is organized as follows: Section 2 describes the inversion model and presents results of sensitivity analysis and the BEC; Section 3 provides details of the WRF-CMAQ model, and configurations and experiments of simulation; Section 4 presents the results of the control and experiment simulations with a *priori* and a constrained *posteriori* ES, respectively; finally, the discussions and conclusions are provided in Section 5.

2. Model and data

We used an offline modeling system that includes two components: the Weather Research and Forecasting (WRF) model (Michalakes et al., 2004) and the CMAQ model (Dennis et al., 1996; hereafter referred to as WRF-CMAQ). This study focuses on the BTH region with 5 x 5-km grid spacing, 32 vertical layers of varying thickness (between the surface and 50 hPa), and an output interval of 1 h. The WRF-CMAQ simulations are driven by the National Center for Environmental Prediction Final (NCEP FNL) analysis data every 6 h during December 27-30, 2016 and the Multi-resolution Emission Inventory for China (MEIC) data for 2012, with 1°×1° and 0.25°×0.25° grid spacing, respectively. The CMAQ model was configured to utilize all layers from the input meteorology. Emissions datasets for CMAQ were generated by the Sparse Matrix Operator Kernel Emissions (SMOKE) model developed by the University of North Carolina (UNC, 2014). Meteorological outputs from the WRF simulations were processed to create model-ready input to CMAQ using the Meteorology-Chemistry Interface Processor (MCIP; Otte al., 2010). The boundary conditions for chemical trace gases consisted of idealized, northern hemispheric, mid-latitude profiles based upon output from the National Oceanic Atmospheric Administration (NOAA) Agronomy Lab Regional Oxidant model. The model simulation started on December 27, 2016. To assess the improved effects of inverse modeling of ES during the heavy haze episode in December 2016, we ran two simulations: a control run with a *priori* MEIC data for 2012, and an experiment run with *a* constrained *posteriori* ES.

Hourly measurements of SO_2, NO_2, and O_3 concentrations at 129 stations during December 27–30, 2016 were obtained from the China National Environmental Monitoring Centre. These data are used to validate simulations from the control and experiment runs. The simulation domains and the locations of the 129 stations are shown in Figure 1.

3. Inverse modeling method

3.1 Constructing BEC matrix

To construct the BEC matrix for the inversion model, we combined the National Meteorological Center's (NMC) technique (Parrish and Derber, 1992) with the SMOKE model based on uncertainty analysis of

the ES inventories. We created the BEC matrix by four steps, as follows:

（1）Determine the total errors of ES from a priori bottom-up inventory.

Uncertainty analyses of ES require detailed information of activities and emission factors from a priori MEIC emission inventory. The relevant data collected in the China Environmental Yearbook are limited, and do not satisfy with the requirements of uncertainty analysis. Therefore, we used the available research results relating to SO_2 and NOx ES, and conducted uncertainty analysis for four types of major sources (industry, power plants, residents, and transportation) based on activities and emission factors from the references (Hong et al.,2017; Zheng et al.,2018; Peng et al.,2019) using the AuvTool Software(Frey et al, 2002), and determining the error ranges in total emission rates of SO_2 and NOx (Table 1). Uncertainties in SO_2 industry and power plant ES are slightly greater than those for NOx, while the opposite is true for emissions from the residential and traffic sectors.

（2）Generate multiple sets of inventories using the random perturbation technique.

Based on the aforementioned error ranges in total emission rates, we generated 30 sets of inventories for SO_2 and NOx with the same resolution as MEIC for each month using a random perturbation method (Kerry et al., 2007). Firstly we obtain the probability distribution of errors of ES based on uncertainty analysis for four sections, respectively. Then we conduct thirty times of random perturbation on uncertainties of four sections of ES according to the probability distributions using the same perturbation coefficients for every perturbation. Lastly we calculate thirty total emission rates using random uncertainties of four sections for every sets of inventories, respectively.

(3) Process the 3-D gridded ES as input to the CMAQ model.

We used the SMOKE model, national population and road network distribution data in 2016, the temporal apportionment coefficients in the BTH region (Zhang et al., 2007, 2009, Simpson et al., 2003, and Wang et al., 2010), and the CB05-ae06-aq chemical species data in the CMAQ model, to process thirty sets of nationwide emission inventories into 3-D gridded ES with a grid spacing of 5×5 km. Each grid has 124×130 points, with 12 vertical levels.

(4) Calculate the BEC matrix of each 3-D gridded ES.

Finally, the NMC method was used to calculate the BEC matrix of the 3-D gridded ES for each month, including horizontal and vertical correlation coefficients and standard deviations. The background error

is defined as the difference between thirty sets of 3-D gridded ES generated by the random perturbation method, and the 3-D gridded background ES directly processed from the original MEIC emission inventory with the SMOKE model, at every hour (24 hours diurnal variation of ES for every month).

According to the literature (Liu et al., 2011; Li et al., 2013; Zang et al., 2016), the approximate calculation of the BEC matrix is as follows:

$$\mathbf{B} \approx \frac{1}{2}\langle (e_t - e_b)(e_t - e_b)^T \rangle, \quad (1)$$

where e_t is the perturbation field and e_b is the background field of *a priori* ES. Eq. (1) can be written as follows:

$$\mathbf{B} = \mathbf{DCD}^{\mathrm{T}}, \quad (2)$$

where **D** is the standard deviation (SD) matrix and **C** is the correlation coefficient matrix. With this factorization, **D** and **C** can be calculated separately. **D** is a diagonal matrix whose elements are SD of all state variables in the 3-D grids. **C** is used to improve the ability of the 3DVAR in representing the impacts of local emissions at one grid on other grids; these impacts vary in the vertical direction, and they are heterogeneous in the horizontal direction.

Figure 2 shows the spatial distribution of averaged emission rates for thirty sets of 3-D gridded ES, and the SD of the BEC matrix for SO_2 and NO_x ES at 08:00 local time in December. SO_2 and NO_x ES have different spatial distributions in terms of average strength and standard deviation. The NO_x emissions are mainly concentrated in cities and surrounding areas, and they are much greater in Beijing, Tianjin, and Shijiazhuang than other cities. The SO_2 emissions are mainly concentrated in Shijiazhuang, Jinan, the north and east of Shanxi Province and their surrounding areas. Figure 3 shows variations in the horizontal correlation coefficients by grid distance, and the vertical distributions of the SD in **B** for SO_2 and NO_x ES in December 2012. The cross between the correlation curve and the $e^{-1/2}$ line (dashed line) represents the horizontal length scale (L_s), and the L_s of the two species falls between five and six grid distances. Namely, the horizontal scale felt is approximately 25–30 km. The correlation coefficient of SO_2 is slightly larger than that of NO_2. The difference in the correlation coefficients between SO_2 and NO_x ES increases with grid distance and this is related to the regional pollution characteristics of SO_2. The vertical distributions of the SDs in **B** for SO_2 and NO_x ES vary with height:

the SD of SO_2 ES are larger on the fourth and eighth model levels than on other levels; while for NO_x ES, the SD on the first level is the largest, that on the eighth level take the second place, and the SDs on all other levels are smaller.

3.2 Sensitivity analysis

The sensitivity analysis module (DDM-3D) in CMAQ solves a series of equations while simultaneously calculating pollutant concentrations. The local sensitivity of pollutant concentrations with respect to several specified parameters, such as ES, initial and boundary conditions, and chemical reaction rates, can be calculated by the DDM-3D method. The sensitivity equations about the ES are solved using the governing equations of the model, as follows (Hu et al., 2009):

$$S_j = p_j \frac{\partial C}{\partial p_j} = p_j \frac{\partial C}{\partial (\varepsilon_j p_j)} = \frac{\partial C}{\partial \varepsilon_j}, \quad (3)$$

where S_j is the sensitivity of the pollutant j to the parameter p_j, p_j is a *priori* ES of the pollutant *j*, *C* is the concentration of the pollutant *j*, and ε_j is the perturbation coefficient of the ES. Theoretically, the DDM-3D method truly captures the sensitivities of pollutant concentrations to ES, and results are more accurate than the brute force method, for the BTH region (Wang et al, 2013). In addition, the results of the DDM-3D method are more accurate and efficient for highly nonlinear pollutants (such as O_3 and $PM_{2.5}$) and small perturbations.

We used the WRFv3.7.1 and CMAQv5.0.2-DDM-3D models as well as 3-D gridded *a priori* ES from MEIC in 2012 to calculate the sensitivity coefficients of SO_2 and NO_2 concentrations with respect to ES during the "heavy haze" episode of December 27–30, 2016. Figure 4 shows the spatial distribution of 96-h averaged sensitivity coefficients for SO_2 and NO_2 concentrations with respect to ES during December 27–30, 2016. The sensitivity coefficients of SO_2 and NO_2 concentrations all exhibit inhomogeneous distribution. The sensitivity coefficients are higher in Beijing, Shijiazhuang, Baoding, and surrounding regions, i.e., SO_2 and NO_2 concentrations in those areas are greatly affected by the SO_2 and NO_x ES.

3.3 Observation operators

The relationship between pollutant source and the receptor's concentration is established according to Eq. (3). Next, we create the observation operator matrix between ES and receptor concentrations as

follows:

$$\mathbf{H} = \frac{\partial \mathbf{C}}{\partial E} = \frac{\partial \mathbf{C}}{\partial(\varepsilon_j E_0)} = \frac{S_j}{E_0}, \quad (4)$$

where **H** is the observation operator matrix, *E* are a *posteriori* ES, which can be written as the product of the perturbation coefficient and *a priori* ES during the assimilation window time, and E_0 are a *priori* ES. For primary pollutants such as SO_2 and NO_2, S_j is a first-order sensitivity coefficient, and **H** is a linear observation operator between the ES and the receptor concentration. For secondary pollutants such as $PM_{2.5}$ and O_3, S_j is a high-order sensitivity coefficient, and **H** is a nonlinear observation operator. In this study, we use the first-order sensitivity coefficient to calculate **H** for SO_2 and NO_x ES.

3.4 Observational error covariance

We firstly performed quality control on the observed SO_2 and NO_2 concentration data. This process involved three steps:

(1) Redundant data removal, and matching the density of observation data to the model grid. For some grids with more than one observation station, we used the average of those stations.

(2) Extrema control, i.e., filtering out data exceeding three times of SD of observation data.

(3) Anomaly removal, i.e., data that remained constant for 24 consecutive hours, as well as any negative data, were removed.

Data that passed quality control still contained observation or instrument errors. These errors are related to many factors such as instrument type, calibration design, and environmental conditions. In addition, in the variational assimilation process, representation errors caused by the forward-calculation and variational processes must be considered. Higher-resolution models produce smaller representation errors. Representation error, ε_r, can be expressed as follows (Pagowski et al., 2010):

$$\varepsilon_r = \gamma \varepsilon_o \sqrt{\frac{\Delta x}{L_s}} \quad (5)$$

where γ is the amplification factor, which is used to adjust the instrument error, ε_o is related to the SO_2 and NO_2 concentrations, and Δx is grid distance of the model. Note that L_s is usually smaller in urban areas and larger in suburban areas. The amplification parameters of the observing stations in cities, suburbs, and rural areas are 2.5 km, 5 km, and 10 km, respectively (Zang et al., 2016). Finally, the total observation error for the SO_2 and NO_2 concentrations, ε, is written as:

$$\varepsilon = \sqrt{\varepsilon_o^2 + \varepsilon_r^2}. \quad (6)$$

3.5 3DVAR inversion model

We introduce a cost function with respect to the ES in accordance with 3DVAR:

$$J(e) = \frac{1}{2}(e - e_b)^T \mathbf{B}^{-1}(e - e_b) + \frac{1}{2}(\mathbf{H}e - c)^T \mathbf{R}^{-1}(\mathbf{H}e - c), \quad (7)$$

where c is the observation variable, $\mathbf{R}$ is the observation error matrix, and e is the inversing variable of an *a posteriori* ES. The optimal inversion of ES for SO_2 and NO_x are obtained using Eq. (7). The 3DVAR solves for the minimum value of $J(e)$ to determine the inversing variable e. This process typically employs a gradient propagation method, with the increment of an ES defined as follows:

$$\delta e = e - e_b, \quad (8)$$

Accordingly, the innovation vector of pollutant concentration is defined as:

$$\delta c = c - \mathbf{H}e_b. \quad (9)$$

Therefore, Eq. (7) can be written in gradient form:

$$J(\delta e) = \frac{1}{2}\delta e^T \mathbf{B}^{-1}\delta e + \frac{1}{2}(\mathbf{H}\delta e - \delta c)^T \mathbf{R}^{-1}(\mathbf{H}\delta e - \delta c). \quad (10)$$

After conditionally processing the cost function, a finite-memory quasi-Newton method was used to conduct iterative minimization. The background field was set as the initial iteration values. The maximum number of steps at the end of the iteration and the minimum gradient for convergence were predetermined. The iteration was finished when one of these conditions was met, and the optimal analysis increment, δe, was obtained. Finally, the optimal assimilation analysis field of the ES, $e = \delta e + e_b$, was obtained. The result was a three-dimensional variational inversion model of the ES, using the uncertainty analysie of the ES and sensitivity coefficients between the ES and receptor's concentrations; the overall framework is shown in Figure 5.

4. Results and discussion

A typical heavy haze event occurred in the BTH region at the end of December 2016. We applied the 3DVAR inversion model to constrain a hourly *posteriori* ES of SO_2 and NO_2 using measurements from 45 and 129 stations, respectively, on December 27, 2016. We validated simulations from the control and experiment run using observational data during December 28–30, 2016.

Figure 6 shows time series of hourly, regional averaged SO_2 and NO_2 simulations from the control run, observations, and sensitivity coefficients at 45 stations in the BTH region during December

27–30, 2016. The trends in modelled concentrations and sensitivity coefficients of SO_2 and NO_2 concentrations with respect to ES are consistent, therefore the sensitivity coefficients can reasonably reflect the impacts of the ES on concentrations. However, simulated SO_2 and NO_2 concentrations with a underestimated *priori* ES are all significantly lower than observations during the heavy haze period. Thus, it is important to improve a *priori* ES using the inversion model.

Figures 7 and 8 show the spatial distributions of 24-h averaged emission rates from a *priori* and *a posteriori* ES of SO_2 and NO_2, and their increments on December 27, 2016. Emission rates of a *posteriori* of SO_2 and NO_2 ES in the major cities and surrounding areas clearly increase. Compared with a *priori* ES, the maximum strengths of SO_2 and NO_2 ES increase by approximately 17% and 500%, respectively. Therefore, the strengths of SO_2 and NO_2 in a *priori* ES were greatly underestimated, especially for NO_2.

Using the WRF-CMAQ model and a *posteriori* ES, we simulated concentrations of SO_2, NO_2, and O_3 in the BTH region during December 28–30, 2016, and validated these simulations with measurements from 45 stations. Figures 9 and 10 show the spatial distributions of 72-h averaged SO_2 and NO_2 concentrations simulated with a *priori* and a *posteriori* ES, increments, and their observations. In general, SO_2 and NO_2 concentrations simulated using a *posteriori* ES are closer to observations than a *priori* ES, and regional differences in improvements for SO_2 and NO_2 exist. For SO_2, the improvement is noticeable in the BTH region. However, the simulated concentrations in Beijing with a *posteriori* ES are overestimated. This may be related to greater uncertainties in SO_2 sources and the impacts of regional transport from surrounding areas. For NO_2, simulated differences with a *priori* and a *posteriori* ES are significant in major cities such as Beijing, Tianjin, Shijiazhuang, Baoding, Xingtai, Handan, and Jinan. The simulated concentrations of NO_2 using a *posteriori* ES are more consistent with measurements, while those with a *priori* ES are significantly underestimated.

We also investigated temporal variations in regionally-averaged SO_2, NO_2, and O_3 concentrations simulated using a *priori* and *a posteriori* ES, and observations from the 45 stations over the BTH region during December 28–30, 2016 (Figure 11). In general, simulated SO_2, NO_2, and O_3 concentrations using a *posteriori* ES are closer to measurements, while the SO_2 and NO_2 concentrations simulated by a *priori* ES are significantly lower than observations, and the modelled O_3 concentrations are obviously

higher than measurements. In addition, the peak of SO_2 simulations with a *posteriori* ES are close to measurements, but the peak of NO_2 and valley of O_3 simulations are lower and higher than observations, respectively. This may be related to the absence of inverse modeling of volatile organic compound (VOC) ES and uncertainties of sensitivity coefficients calculation. In this study, we used only first-order sensitivity coefficients, but the relationship between ES of precursors of O_3 such as VOCs and NOx, and their receptor's concentrations are nonlinear, and O_3 is generated from both NOx and VOCs ES. Therefore, higher-order sensitivity coefficients are necessary for inverse modeling of ES of NOx and VOCs.

To further assess the simulated accuracy of SO_2, NO_2, and O_3 concentrations, we calculated the following statistics (Willmott et al., 2011): correlation coefficient (R), root-mean-squared error (RMSE), mean bias (MB), normalized mean bias (NMB), and index of agreement (IOA; see Table 2). Except that R of NO_2 and O_3 decrease and RMSE of O_3 increases using the constrained ES, other statistics show improvements. Especially, MB and NMB of three pollutants decline significantly and IOA are closer to 1.0, which means that modelled results of three pollutants are more consistent with observations. R between SO_2 simulation and observation shows a slight improvement when using a *posteriori* ES, whereas R decreases for NO_2 and O_3, and it may be related with the absence of constraint of VOCs ES.

5. Summary and conclusions

We developed a new inverse approach of ES by combining the sensitivity analysis technique between ES and receptor's concentration, and the 3DVAR method. Our approach is suitable for solving the linear or nonlinear inversion problems for ES, and it compute fastly and obtain the relatively accurate real-time dynamic updates of ES. First, we used the sensitivity analysis tool in the CMAQ model to construct the explicit observation operator matrix between ES and receptor's concentration. Next, we created the BEC matrix for ES based on uncertainty analysis and the NMC statistical method. Finally, we established a three-dimensional variational inverse method of ES based on the observation operator and BEC matrix.

The 3DVAR inversion model was applied to a heavy haze case study in the BTH region during December 27–30, 2016. Results show that the observation operators between SO_2 and NO_2 ES, and their concentrations, as well as spatial distributions of the BEC matrix are both reasonable. Using the

3DVAR inversion model, a *priori* SO_2 and NO_2 ES improved obviously during the heavy haze process, especially for NO_2 ES. The spatial distributions of SO_2 and NO_2 concentrations simulated using a *posteriori* ES are more consistent with measurements than a *priori* ES, especially in major cities over the BTH region. Simulation errors of SO_2, NO_2 and O_3 concentrations with a *posteriori* ES significantly decrease, whereas simulations of three pollutants using a *priori* ES are underestimated.

Large discrepancies of the simulation and sensitivity coefficient over December 29 may be related with absent calculation of high-order sensitivity coefficient in this case. In the future, we will adopt high-order sensitivity coefficient to improve the constraint effect of SO_2 and NO_x emission sources. In addition, future studies will include the applicability and accuracy of this method for different seasons and regions, and different chemical species such as other primary pollutants (e.g., CO) and precursors of secondary pollutants (e.g., $PM_{2.5}$, PM_{10} and O_3). An emphasis may be placed on constructing the nonlinear explicit observation operator for precursors of secondary pollutants such as VOCs ES using the high-order sensitivity analysis technique, and assessing improvement effects of a *posteriori* ES with the 3DVAR inversion method and CMAQ model.

Data availability. The NCEP-FNL reanalysis data are publicly available at http://rda.ucar.edu/datasets/ds083.2/. The SO_2, NO_2, and O_3 measurements are available at http://113.108.142.147:20035/emcpublish.

Author contributions. XC and ZZ designed the research. XC and ZH constructed the 3DVAR inversion model, designed model experiments and performed simulations. XC, ZH, ZZ, YL, YH and XM contributed to the data processing and analyses. XC and ZH analyzed the results and wrote the paper with inputs from all authors. ZL and XX contributed to theoretical direction for establishing the inversion model. SW performed the uncertainty analysis of ES.

Competing interests. The authors declare that they have no conflicts of interest.

Acknowledgements. We are grateful to Tsinghua University for providing the emission inventory and the China National Environmental Monitoring Centre for providing surface SO_2, NO_2, and O_3 observation data.

Financial support. This work was supported jointly by the Fundamental Research Funds for Central Public-interest Scientific Institution from Chinese Academy of Meteorological Sciences (grant no. 2016Y005), the National Natural Science Foundation of China (grant no. 91644223), and the National

Research Program for Key Issues in Air Pollution Control (grant no. DQGG0104).

References

Bai, N. B., Zhou, X. J.: Estimation of CO2, SO2 and NOx gridded emission sources with a resolution of 1°×1° in Changes of atmospheric ozone and its impact on climate and environment in China, Beijing: China Meteorological Press,145-150,1996.

Barbu, A. L., Segers, A. J., Schaap, M., Heemink, A. W., Builtjes, P. J. H.: A multi-component data assimilation experiment directed to sulphur dioxide and sulphate over Europe, Atmos. Environ., 43 (9), 1622-1631, 2009.

Bergamaschi, P., Hein, R., Heimann, M., Crutzen, M., P. J.: Inverse modeling of the global CO cycle: 1. Inversion of CO mixing ratios, J. Geophys. Res.,105(D2), 1909–1927, 2000.

Cao, G. L., Zhang, X. Y., Gong, S. L., Gong, S. L., An, X. Q., Wang, Y.Q.: Emission inventories of primary particles and pollutant gases for China, Chin. Sci. Bull., 56, doi:10.1007/s11434-011-4373-7, 2011.

Cheng, X., Xu, X., Ding, G.: An emission source inversion model based on satellite data and its application in air quality forecasts, Science China: Earth Sciences, 53, 752-762, 2010.

Cheng, Y. F., Zheng, G. J., Wei, C., Mu, Q., Zheng, B., Wang, Z. B, Gao, M., Zhang, Q., He, K. B., Carmichael, G., Pöschl, U., Su, H.: Reactive nitrogen chemistry in aerosol water as a source of sulfate during haze events in China, Sci. Adv., 2, e1601530, 2016.

Chen, D., Liu, Z., Ban, J., and Chen, M.: The 2015 and 2016 wintertime air pollution in China: SO2 emission changes derived from a WRF-Chem/EnKF coupled data assimilation system, Atmos. Chem. Phys., 19, 8619–8650, https://doi.org/10.5194/acp-19-8619-2019 , 2019.

Cohan, D., Hu, Y., Hakami, A., Odman, M. T., Russell, A.: Implementation of a direct sensitivity method into CMAQ, Models-3 User's Workshop, RTP, North Carolina, October 22, 2002.

Corazza, M., Bergamaschi, P., Vermeulen, A. T., Aalto, T.: Inverse modelling of European N2O emissions: Assimilating observations from different networks, Atmos. Chem. Phys., 11 (5), 2381-2398, 2011.

Dai, T., Cheng, Y. M., Goto, D., Li, Y. R., Tang., X., Shi, G. Y., Nakajima, T.: Revealing the sulfur

dioxide emission reductions in China by assimilating surface observations in WRF-Chem, Atmos. Chem. Phys., 21, 4357–4379, https://doi.org/10.5194/acp-21-4357-2021, 2021.

Dennis, R., Byun, D., Novak, J.:The next generation of integrated air quality modeling: EPA's Models-3, Atmos. Environ., 30, 1925-1938,1996.

Elbern, H., Schmidt, H., Talagrand, O., Ebel, A.: 4D-variational data assimilation with an adjoint air quality model for emission analysis, Environmental Modelling & Software, 15 (6), 539-548, 2000.

Elbern, H., Strunk, A., Schmidt, H., Talagrand, O.: Emission rate and chemical state estimation by 4-dimensional variational inversion, Atmos. Chem. Phys., 7, 3749-3769, 2007.

Enting, I. G.: Inverse Problems in Atmospheric Constituent Transport, Cambridge: Cambridge University Press, 2002.

Frey, H.C., Zheng, J., Zhao, Y., Li, S., Zhu, Y.: Technical Documentation of the AuvTool Software for Analysis of Variability and Uncertainty, Prepared by North Carolina State University for the Office of Research and Development, U.S. Environmental Protection Agency, Research Triangle Park, NC. February 2002

Gilliland, A. B., Dennis, R. L., Roselle, S. J., Pierce, T. E.: Seasonal NH3 emission estimates for the eastern United States based on ammonium wet concentrations and an inverse modeling method, J. Geophys. Res., 2003, 108(D15), 4477, doi:10.1029/2002JD003063, 2003.

Gilliland, A. B., Wyat, A. K., Pinder, R. W., Dennis, R. L.: Seasonal NH3 emissions for the continental united states: Inverse model estimation and evaluation, Atmos. Environ., 40 (26), 4986-4998, 2006.

Heald, C. L., Jacob, D. J., Jones, D. B. A., Palmer, P. I., Logan, J. A., Streets,D. G., Sachse, G. W., Gille, J. C., Hoffman, R. N., Nehrkorn, T.: Comparative inverse analysis of satellite (MOPITT) and aircraft (TRACE-P) observations to estimate Asian sources of carbon monoxide, J. Geophys. Res., 2004, 109, D23306, doi:10.1029/2004JD005185,2004.

Henze, D. K., Seinfeld, J. H., Shindell, D. T.: Inverse modeling and mapping US air quality influences of inorganic PM2.5 precursor emissions using the adjoint of GEOS-Chem, Atmos. Chem. Phys., 9, 5877-5903, 2009.

Hong, C., Zhang, Q., He, K., Guan, D., Li, M., Liu, F., Zheng, B.: Variations of China's emission estimates: response to uncertainties in energy statistics, Atmos. Chem. Phys., 17, 1227-1239, 2017.

Hu, Y., Odman, M.T., Russell, A.G.: Top-down analysis of the elemental carbon emissions inventory in the United States by inverse modeling using Community Multiscale Air Quality model with decoupled direct method (CMAQ-DDM), J. Geophys. Res., 114, D24302, doi: 10.1029/2009JD011987, 2009.

Huang, R. J., Zhang, Y., Bozzetti, C., Ho, K. F., Cao, J. J., Han, Y., Daellenbach, K. R., Slowik, J. G., Platt, S. M., Canonaco, F., Zotter, P., Wolf, R., Pieber, S. M., Bruns, E. A., Crippa, M., Ciarelli, G., Piazzalunga, A., Schwikowski, M., Abbaszade, G., Schnelle-Kreis, J., Zimmermann, R., An, Z., Szidat, S., Baltensperger, U., Haddad, I. E., Prévôt, A. S.: High secondary aerosol contribution to particulate pollution during haze events in China, Nature, 514, 218–222, 2014.

Jiang, Z., Jones, D.B.A., Kopacz, M., Liu, J., Henze,D. K., Heald, C.: Quantifying the impact of model errors on top-down estimates of carbon monoxide emissions using satellite observations, J. Geophys. Res., 116, D15306,2011.

Kerry, A., Gerhard, R., Mike, D. F.: Fire-growth modelling using meteorological data with random and systematic perturbations, International Journal of Wildland Fire, 16(2),174-182, 2007.

Koohkan, M. R., Bocquet, M., Roustan, Y., Kim, Y., Seigneur, C.: Estimation of volatile organic compound emissions for Europe using data assimilation, Atmos. Chem. Phys., 13 (12), 5887-5905, 2013.

Kopacz, M., Jacob, D.J., Henze, D.K., Heald, C. L., Streets, D. G., Zhang, Q.: Comparison of adjoint and analytical Bayesian inversion methods for constraining Asian sources of carbon monoxide using satellite (MOPITT) measurements of CO columns. J. Geophys. Res., 114, D04305, 2009.

Li, M., Liu, H., Geng, G., Hong, C., Liu, F., Song, Y., Tong, D., Zheng, B., Cui, H., Man, H., Zhang, Q., He, K.: Anthropogenic emission inventories in China: a review, National Science Review, 4, 834-866, 2017.

Li, Z., Zang, Z., Li, Q.B., Chao, Y., Chen, D., Ye, Z., Liu, Y., Liou, K.N.: A three dimensional variational data assimilation system for multiple aerosol species with WRF/Chem and an application to PM2.5 prediction, Atmos. Chem. Phys., 13, 4265-4278, 2013.

Liu, F., Hu, F., Zhu, J.: Solving the optimal layout problem of multiple industrial pollution sources using the adjoint method, Science China: Earth Sciences, 35 (1), 64-71, 2005.

Liu, J., Mauzerallb, D. L., Chen. Q., Zhang, Q., Song, Y., Peng, W., Klimont, Z., Qiu, X.H., Zhang, S.Q., Hu, M., Lin, W. L., Smith, K. R., and Zhu, T.: Air pollutant emissions from Chinese households: A major and underappreciated ambient pollution source, Proc. Natl. Acad. Sci. USA, 113 (28), 7756-7761, 2016.

Liu, Z., Liu, Q., Lin, H. C., Schwartz, C.S., Lee, Y. H., Wang, T.: Three-dimensional variational assimilation of MODIS aerosol optical depth: implementation and application to a dust storm over East Asia, J. Geophys. Res., 116, D23206, 2011.

Ma, J., Aardenne, J. A. V.: Impact of different emission inventories on simulated tropospheric ozone over China: a regional chemical transport model evaluation, Atmos. Chem. Phys., 4, 877-887, 2004.

Manning, A. J., Doherty, S. O., Jones, A. R., Simmonds, P. G., Derwent, R. G.: Estimating UK methane and nitrous oxide emissions from 1990 to 2007 using an inversion modeling approach, J. Geophys. Res., 116, D02305, doi:10.1029/2010JD014763, 2011.

Martin, R.V., Jacob, D.J., Chance, K., Palmer,P.I ., Evans, M.J.: Global inventory of nitrogen oxide emissions constrained by space-based observations of NO2 columns, J. Geophys. Res., 108, 4537, 2003.

,Michalakes, J., J. Dudhia, D. Gill, T. Henderson, J. Klemp, W. Skamarock, W. Wang.: The Weather Reseach and Forecast Model: Software Architecture and Performance, Proceedings of the 11th ECMWF Workshop on the Use of High Performance Computing In Meteorology, 25-29 October 2004, Reading U.K. Ed. George Mozdzynski, 2004.

Mijling, B., Van, der, A R J.: Using daily satellite observations to estimate emissions of short-lived air pollutants on a mesoscopic scale, J. Geophys. Res., 117 (D17), D17302, doi:10.1029/2012JD017817, 2012.

Miyazaki, K., Eskes, H. J., Sudo, K.: Global NOx emission estimates derived from an assimilation of OMI tropospheric NO2 columns, Atmos. Chem. Phys., 12, 2263-2288, 2012.

Napelenok, S. L., Pinder, R. W., Gilliland, A. B., Martin, R. V.: A method for evaluating spatially resolved NOx emissions using Kalman filter inversion, direct sensitivities, and space-based NO2observations, Atmos. Chem. Phys., 8, 5603-5614, 2008.

Otte, T. L., Pleim, J. E.: The Meteorology-Chemistry Interface Processor (MCIP) for the CMAQ

modeling system: updates through MCIPv3.4.1, Geosci. Model Dev., 3, 243-256, 2010.

Pagowski, M., Grell, G.A., McKeen, S.A., Peckham, S.E., Devenyi, D.: Threedimensional variational data assimilation of ozone and fine particulate matter observations: some results using the weather research and forecasting-chemistry model and grid-point statistical interpolation, Q. J. R. Meteorol. Soc., 136, 2013-2024, 2010.

Parrish, D.F., Derber, J.C.: The National Meteorological Center's spectral statisticalinterpolation analysis scheme, Mon. Weather Rev., 120, 1747-1763,1992.

Peng, Z., Liu, Z., Chen, D., Ban, J. M.: Improving PM2.5 forecast over China by the joint adjustment of initial conditions and source emissions with an ensemble Kalman filter, Atmos. Chem. Phys., 17 (7), 4837-4855, 2017.

Peng, L., Zhang, Q., Yao, Z., Mauzerall, D. L., Kang, S., Du, Z., Zheng, Y., Xue, T., He, K.: Underreported coal in statistics: A survey-based solid fuel consumption and emission inventory for the rural residential sector in China, Appl. Energ., 235, 1169-1182, 2019.

Sportisse, B.: A review of current issues in air pollution modeling and simulation, Computational Geosciences, 11 (2), 159-181, 2007.

Stavrakou, T., Müller, J. F., De, S. I., Roozendael, V.: The continental source of glyoxal estimated by the synergistic use of spaceborne measurements and inverse modeling, Atmos. Chem. Phys., 9 (21), 8431-8446, 2009.

Streets, D. G., Bond, T. C., Carmichael, G. R., Fernandes, S.D.,Fu, Q.,He, D. Klimont Z., Nelson, S.M.,Tsai, N.Y.,Wang, M.Q.,Woo, J.H., Yarber, K.F.: An inventory of gaseous and primary aerosol emissions in Asia in the year 2000, J. Geophys. Res., 108(D21), 8809-8820, 2003.

Tang X, Zhu J, Wang Z F, Gbaguidi, A.: Improvement of ozone forecast over Beijing based on ensemble Kalman filter with simultaneous adjustment of initial conditions and emissions, Atmos. Chem. Phys.,11 (24), 12901-12916,2011.

Tang, X., Zhu, J., Wang, Z. F., Gbaguidi, A., Lin, C. Y., Xin, J. Y., Song, T., Hu, B.: Limitations of ozone data assimilation with adjustment of NOx emissions: Mixed effects on NO2 forecasts over Beijing and surrounding areas, Atmos. Chem. Phys., 16 (10), 6395-6405, 2016.

Tang, X.Y., Zhang, Y. H., Shao, M.: Atmospheric Environmental Chemistry (second edition) (Chin.

Ver.). Beijing: Higher Education Press, 447-449, 2006.

The University of North Carolina.: SMOKE v3.6 user's manual, Chapel Hill: The institute for the Environment, 1-520, 2014.

Wang, C., An, X. Q., Zhai, S. X., Hou, Q., Sun, Z. B.: Tracking sensitive source areas of different weather pollution types using GRAPES-CUACE adjoint model, Atmos. Environ., 175, 154-166, 2018.

Wang, L. T., Zhang, P., Yang, J., Zhao, X. J., Wei, W., Su, J., Cheng, D. D., Liu X., Y., Han, G., G., Wang, H. J.: Application of CMAQ-DDM-3D in the source analysis of fine particulate matter ($PM_{2.5}$), Acta. Scientiae Circumstantiae (Chin. Ver.), 33(5),1355-1361, 2013.

Wang, P., Wang, H., Wang, Y. Q., Zhang, X. Y., Gong, S. L., Xue, M., Zhou, C. H., Liu, H. L., An, X. Q., Niu, T., Cheng, Y. L.: Inverse modeling of black carbon emissions over China using ensemble data assimilation, Atmos. Chem. Phys., 16 (2), 989-1002, 2016.

Wang, Y. S., Yao, L., Wang, L., L., Liu, Z. R., Ji, D. S., Tang, G. Q., Zhang, J. K., Sun, Y., Hu, B., Xin, J. Y.: Mechanism for the formation of the January 2013 heavy haze pollution episode over central and eastern China, Science China. Earth Sciences (Chin. Ver.), 57, 14-25, 2014.

Wang, Y., McElroy, M. B., Martin, R. V., Streets, D. G., Zhang, Q., Fu, T.-M.: Seasonal variability of NOx emissions over east China constrained by satellite observations: Implications for combustion and microbial sources, J. Geophys. Res., 112, D06301, doi,10.1029/2006JD007538, 2007.

Willmott, C. J., Robeson, S. M. and Matsuura, K. A.: A refined index of model performance, International Journal of Climatology, 32, 2088-2094, 2012.

Xu, X. D., Xie, L. A., Cheng, X. H., Xu., J. M., Zhou, X. J., Ding, G. A.: Application of an Adaptive Nudging Scheme in Air Quality Forecasting in China, J. Appl. Meteorol. Climatol., 47, 2105-2114, 2008.

Yang, Q., Wang, Y. H., Zhao, C., Liu, Z., William, I., Gustafson, J., Shao, M.: NOX emission reduction and its effects on ozone during the 2008 Olympic Games, Environ. Sci. Technol., 45 (15), 6404-6410, 2011.

Zang, Z. L., Li, Z.J., Pan, X.B., Hao, Z.L., You, W.: Aerosol data assimilation and forecasting experiments using aircraft and surface observations during CalNex, Tellus B, 68, 29812,2016.

Zhang, L., Shao, J. Y., Lu, X., Zhao, Y. H., Hu, Y. Y., Henze,D., Liao, H., Gong, S., L., Zhang, Q.:

Sources and processes affecting fine particulate matter pollution over North China: An adjoint analysis of the Beijing APEC period, Environ. Sci. Technol., 50 (16), 8731-8740, 2016.

Zhang, Q., G. N. Geng, S. W. Wang, S.W., Andreas, R., HE, K. B.: Satellite remote sensing of changes in NOx emissions over China during 1996-2010, Chin. Sci. Bull., 57, 2857-2864, 2012.

Zhang, Q., Streets, D.G., Carmichael, G.R., He, K. B., Huo, H., Kannari, A., Klimont, Z., Park, I. S., Reddy, S., Fu, J. S., Chen, D., Duan, L., Lei, Y., Wang, L. T., Yao Z. L.: Asian emissions in 2006 for the NASA INTEX-B mission, Atmos. Chem. Phys., 9, 5131-5153, 2009.

Zhao, B., Wang, P., Ma, J. Z., Zhu, S., Pozzer, A., Li, W.: A high-resolution emission inventory of primary pollutants for the Huabei region, China, Atmos. Chem. Phys., 12, 481-501, 2012.

Zhao, H. Y., Zhang, Q., Guan, D. B., Davis, S. J., Liu, Z., Huo, H., Lin, J. T., Liu, W. D., He, K. B.: Assessment of China's virtual air pollution transport embodied in trade by using a consumption-based emission inventory, Atmos. Chem. Phys., 15(10), 5443-5456, 2015.

Zheng, B., Tong, D., Li, M., Liu, F., Hong, C., Geng, G., Li, H., Li, X., Peng, L., Qi, J., Yan, L., Zhang, Y., Zhao, H., Zheng, Y., He, K., Zhang, Q.: Trends in China’s anthropogenic emissions since 2010 as the consequence of clean air actions, Atmos. Chem. Phys., 18, 14095-14111, 2018.

Zhu, J., Tang, X., Wang, Z. F., Wu, L.:A review of air quality data assimilation methods and their application, Chinese Journal of Atmospheric Sciences, 42 (3), 607-620, 2018.

Zhu, J., Wang, P.: Ensemble kalman smoother and ensemble kalman filter approaches to the joint air quality state and emission estimation problem, Chinese Journal of Atmospheric Sciences, 30(5), 871-882, 2006.

Table 1. Uncertainty of NO_x and SO_2 values used in the SMOKE model and calculation of the BEC matrix.

Categories	NO_x	SO_2
Industry	(−32.4%, 33.0%)	(−37.5%, 38.8%)
Power	(−32.4%, 33.0%)	(−37.5%, 38.8%)
Residential	(−30.0%, 34.0%)	(−15.0%, 16.0%)
Transportation	(−55.4%, 70.3%)	(−17.0%, 20.0%)

Table 2. Statistics for simulated SO_2, NO_2, and O_3 from control and experiment runs using a *priori* and *a posteriori* inversed ES at 45 stations in the BTH region during December 28–30, 2016. Bold type indicates better statistical results.

Parameters	Control Run			Experiment Run		
	SO_2	NO_2	O_3	SO_2	NO_2	O_3
R	0.80	0.82	0.89	**0.82**	0.52	0.87
RMSE	14.61	8.89	5.02	**6.60**	**8.68**	6.31
MB	-40.98	-48.20	26.91	**3.23**	**-2.23**	**4.70**
NMB	-0.61	-0.81	1.78	**0.05**	**-0.04**	**0.31**
IOA	0.42	0.27	0.45	**0.89**	**0.68**	**0.84**

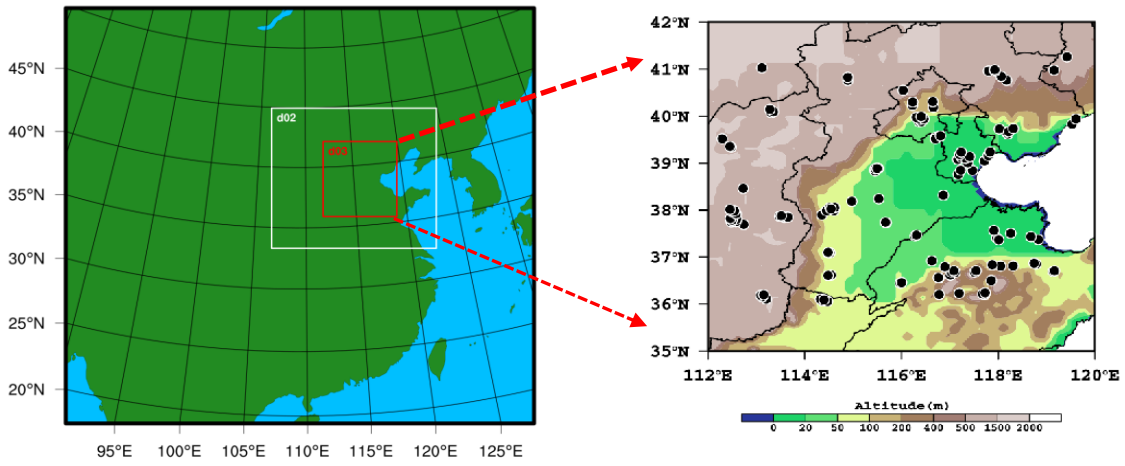

Figure 1 (a) Domain of the WRF-CMAQ model and **(b)** location of environmental monitoring stations in the innermost domain over the BTH region.

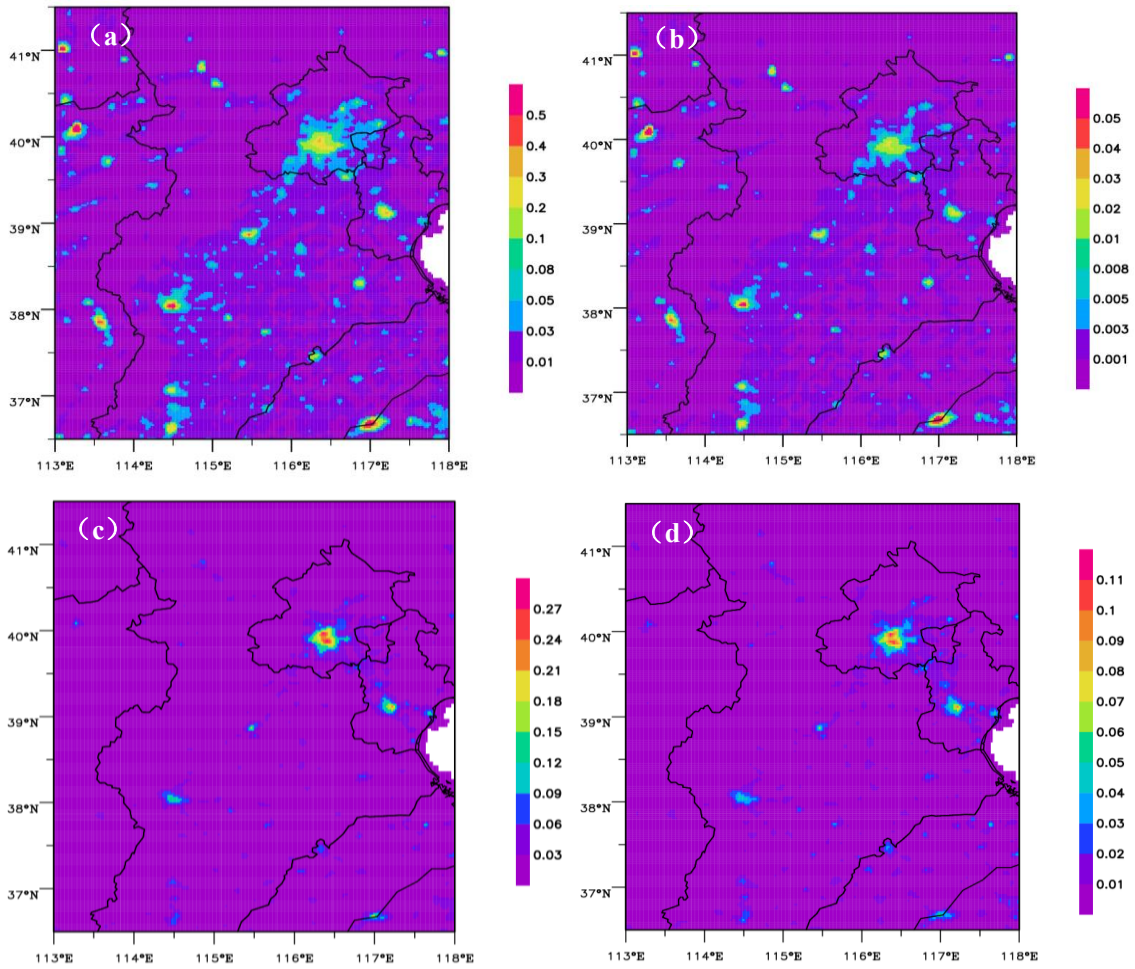

Figure 2 Spatial distributions of **(a)** averaged emission rates of SO_2 ES, **(b)** standard deviation in the BEC of SO_2 ES, **(c)** averaged emission rates of NOx ES, **(d)** standard deviation in the BEC of NOx ES at 08:00 local time in December 2012. Unit: mole/s.

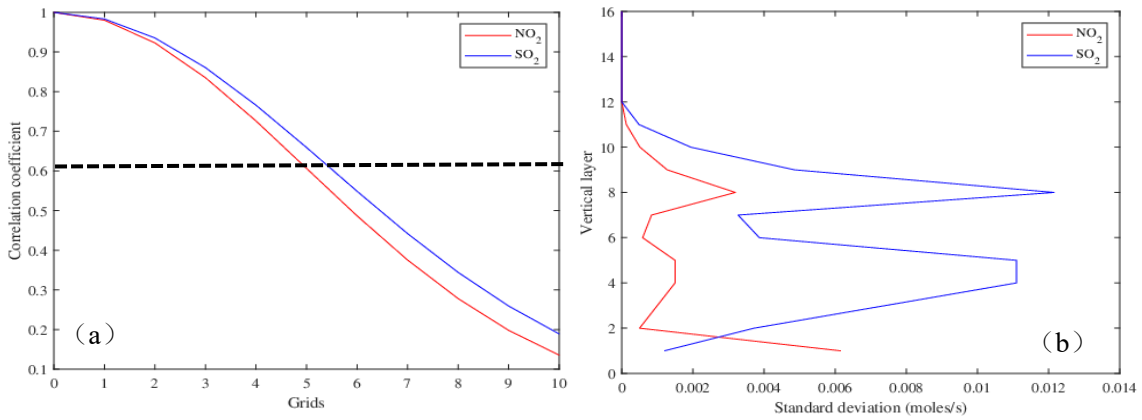

Figure 3 (a) Horizontal correlation coefficients with increasing grid distance, and **(b)** vertical profiles of standard deviations in the BEC of SO_2 and NO_2 ES in December 2012. Dashed line is the baseline of horizontal correlation scale.

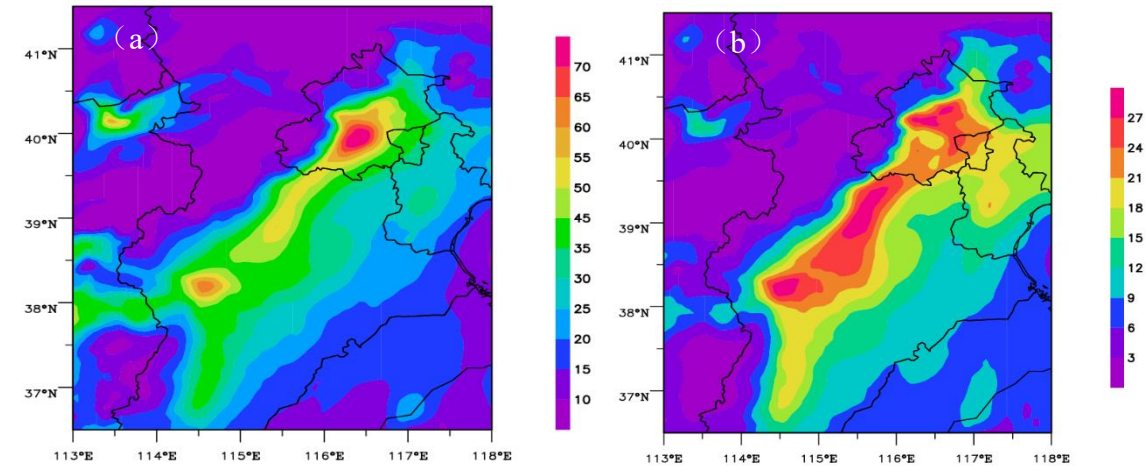

Figure 4 Spatial distributions of 96-h averaged sensitivity coefficients (μg m^{-3}) of **(a)** SO_2 and **(b)** NO_x concentrations with respect to SO_2 and NOx ES during December 27–30, 2016.

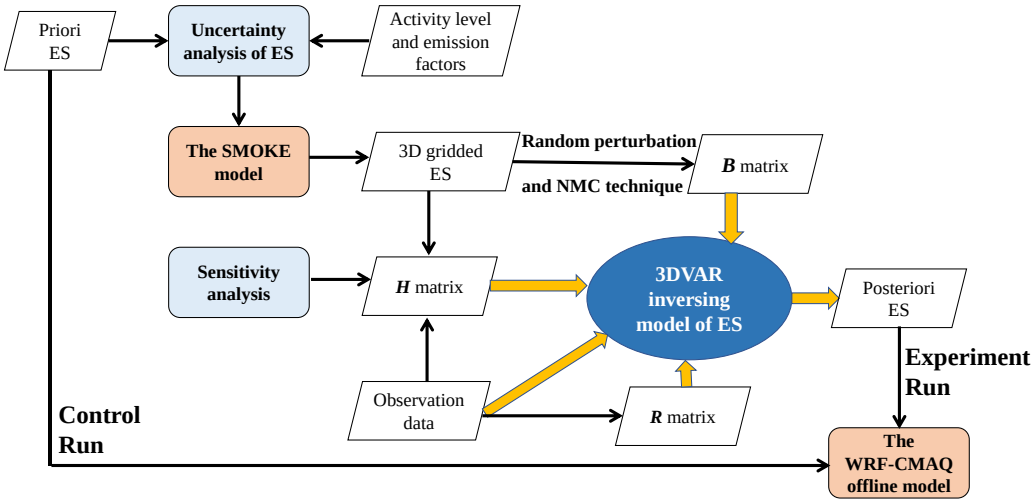

Figure 5 Flowchart of the 3DVAR inversion model of ES and simulation experiments.

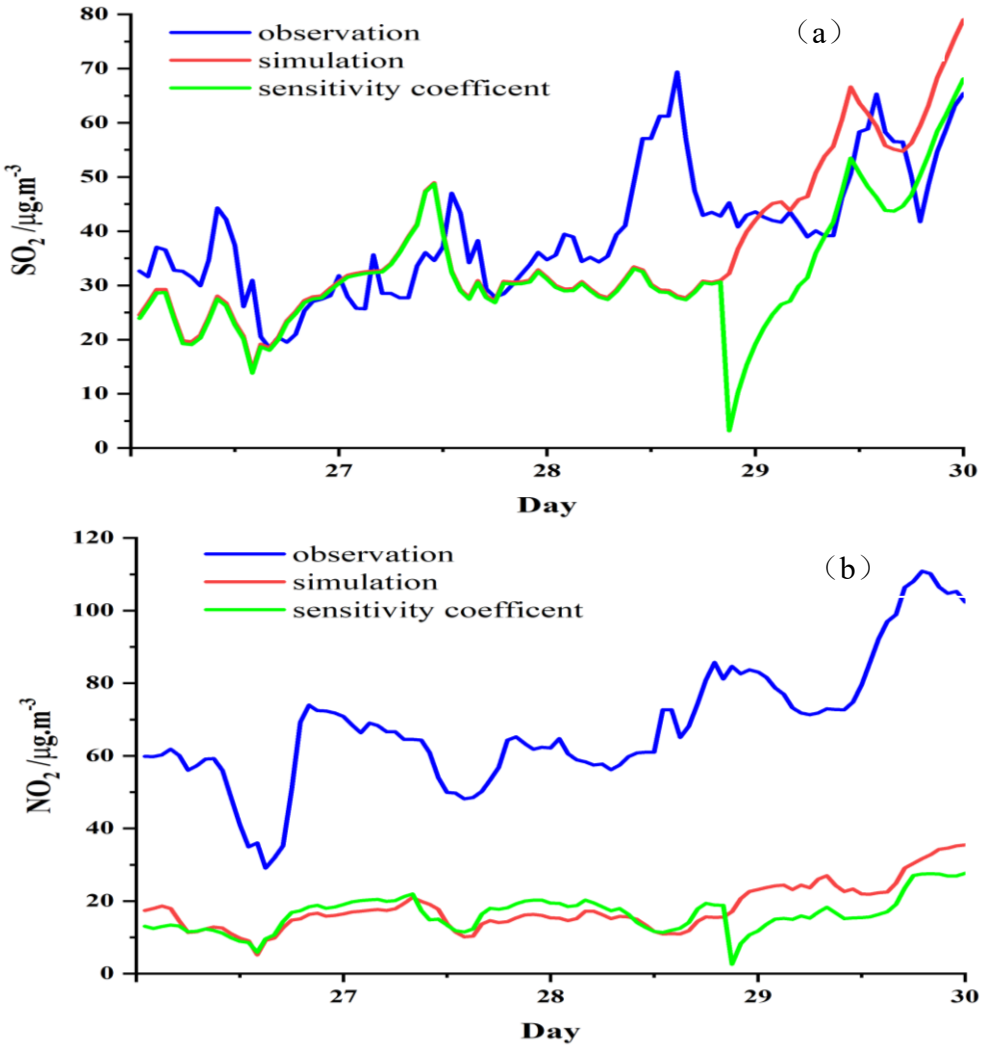

Figure 6 Time series of hourly, regionally-averaged **(a)** SO_2 and **(b)** NO_2 simulations with a *priori* ES, observations, and the first-order sensitivity coefficients between the ES and receptor's concentration at 45 stations over the BTH region during December 27-30, 2016.

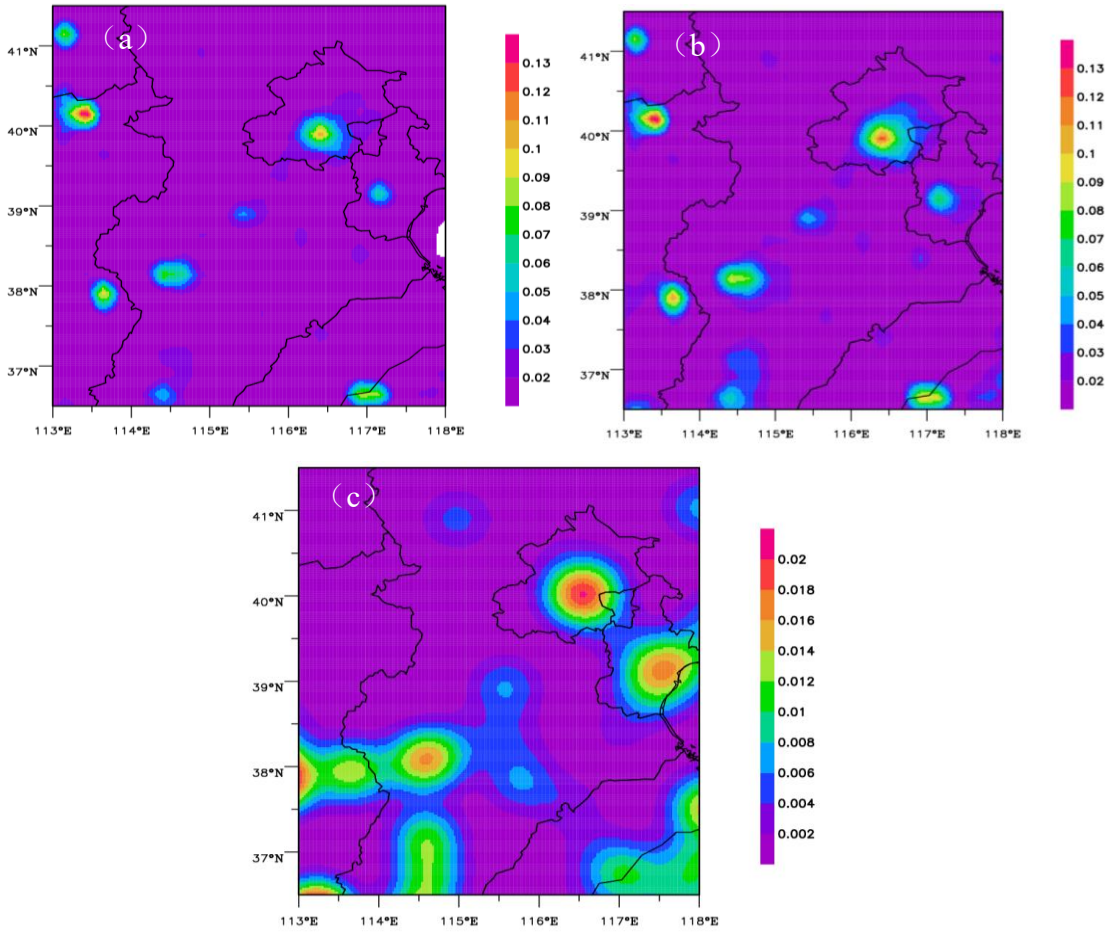

Figure 7 Spatial distributions of 24-h averaged emission rates for SO_2 (mole/s) from **(a)** *a priori* and **(b)** a *posteriori* ES, and **(c)** the increment on December 27, 2016.

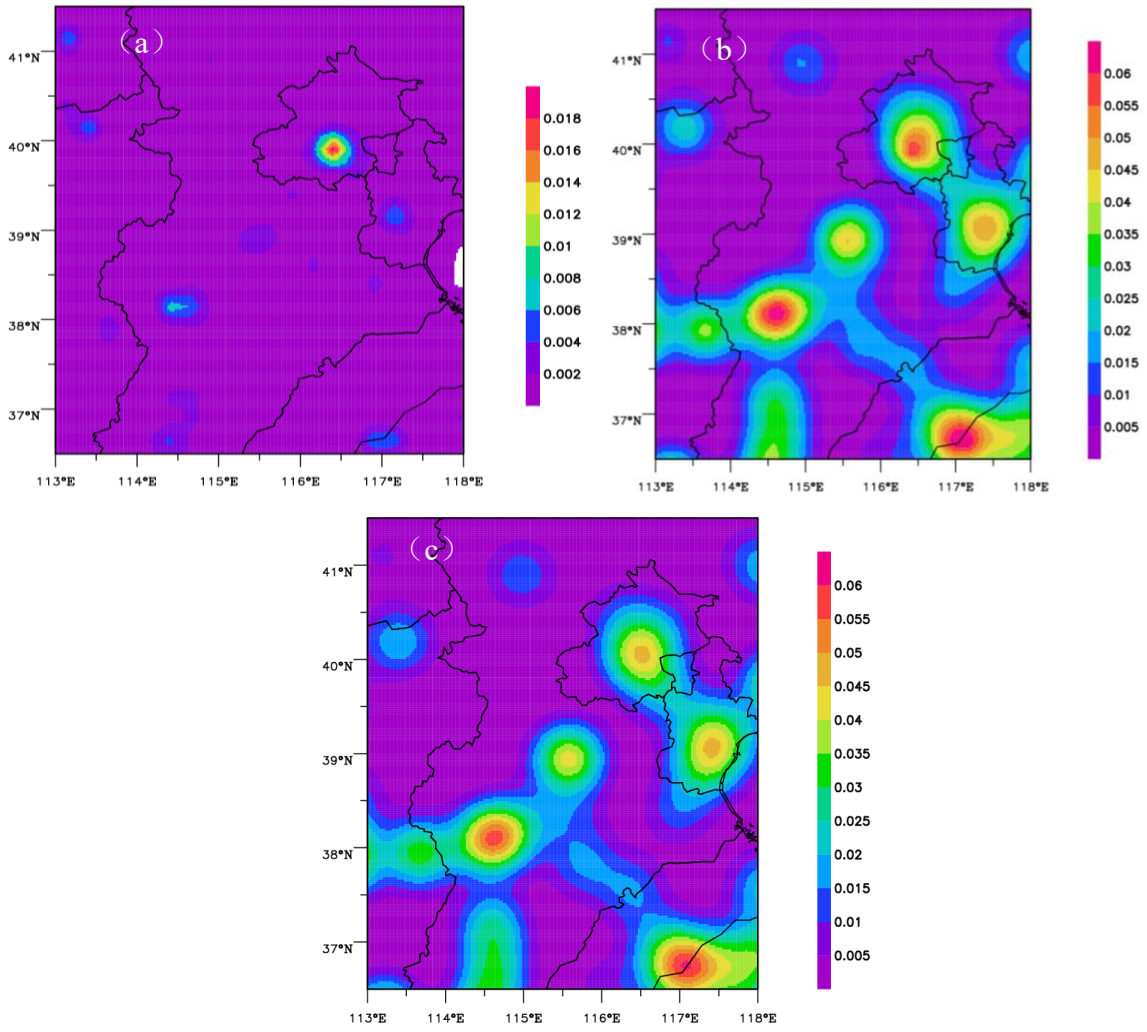

Figure 8 Same to Fig.7 except for NO_2.

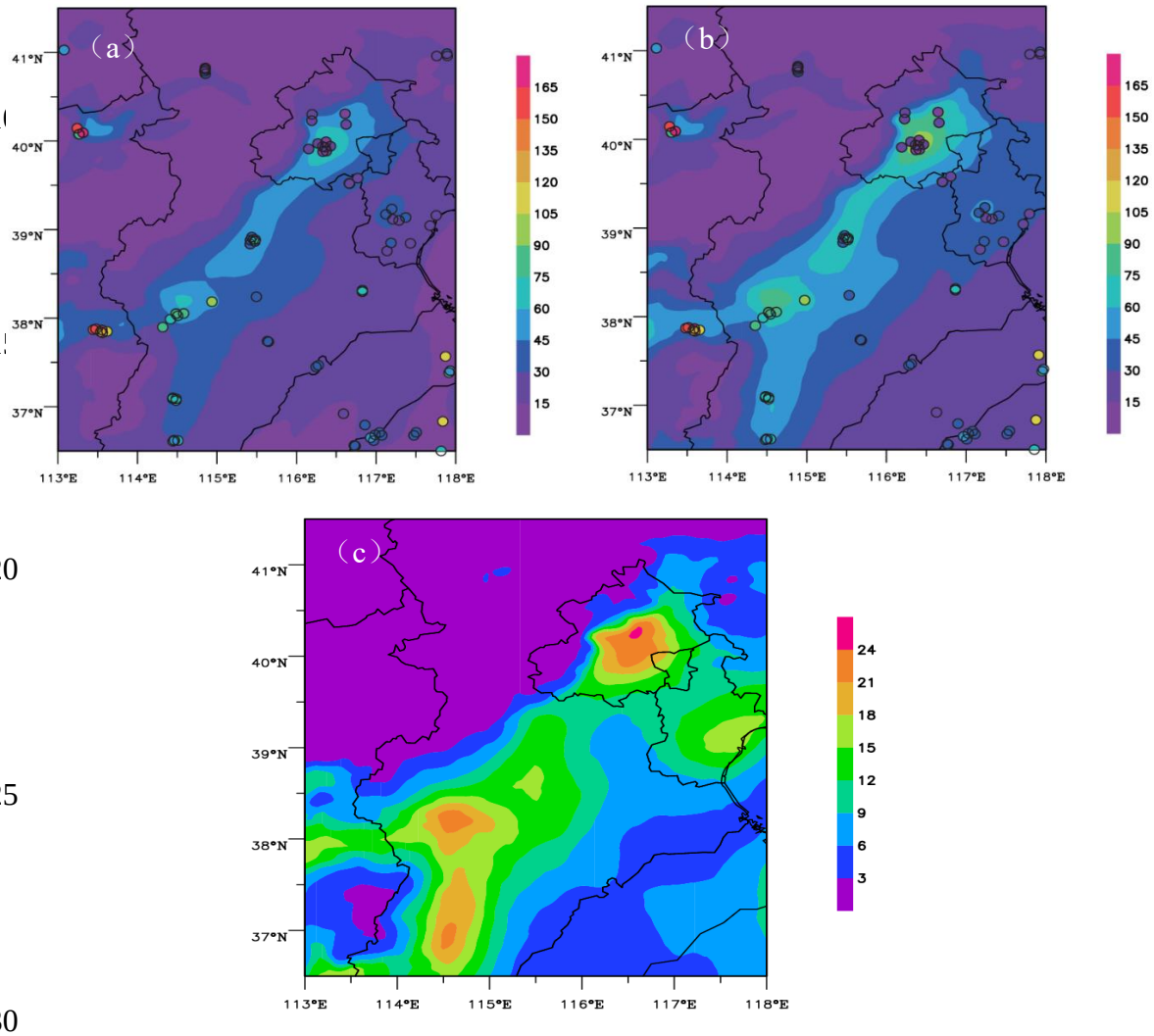

Figure 9 Spatial distribution of 72-h averaged SO_2 concentration simulated with **(a)** *a priori* and **(b)** a *posteriori* ES, and **(c)** the increment during December 28-30, 2016. Color solid dot denotes the measurements.

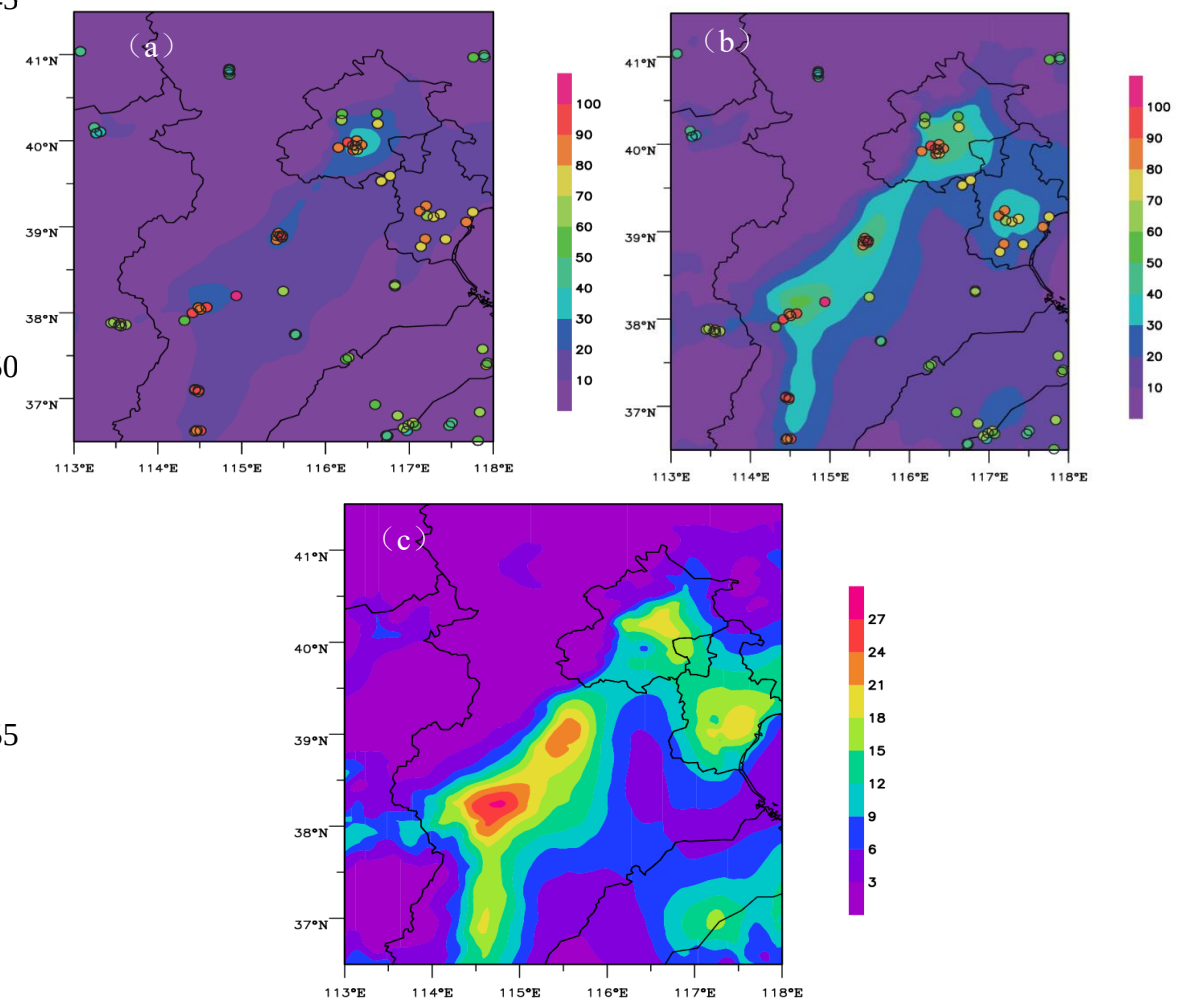

Figure 10 Same to Fig.9 except for NO_2.

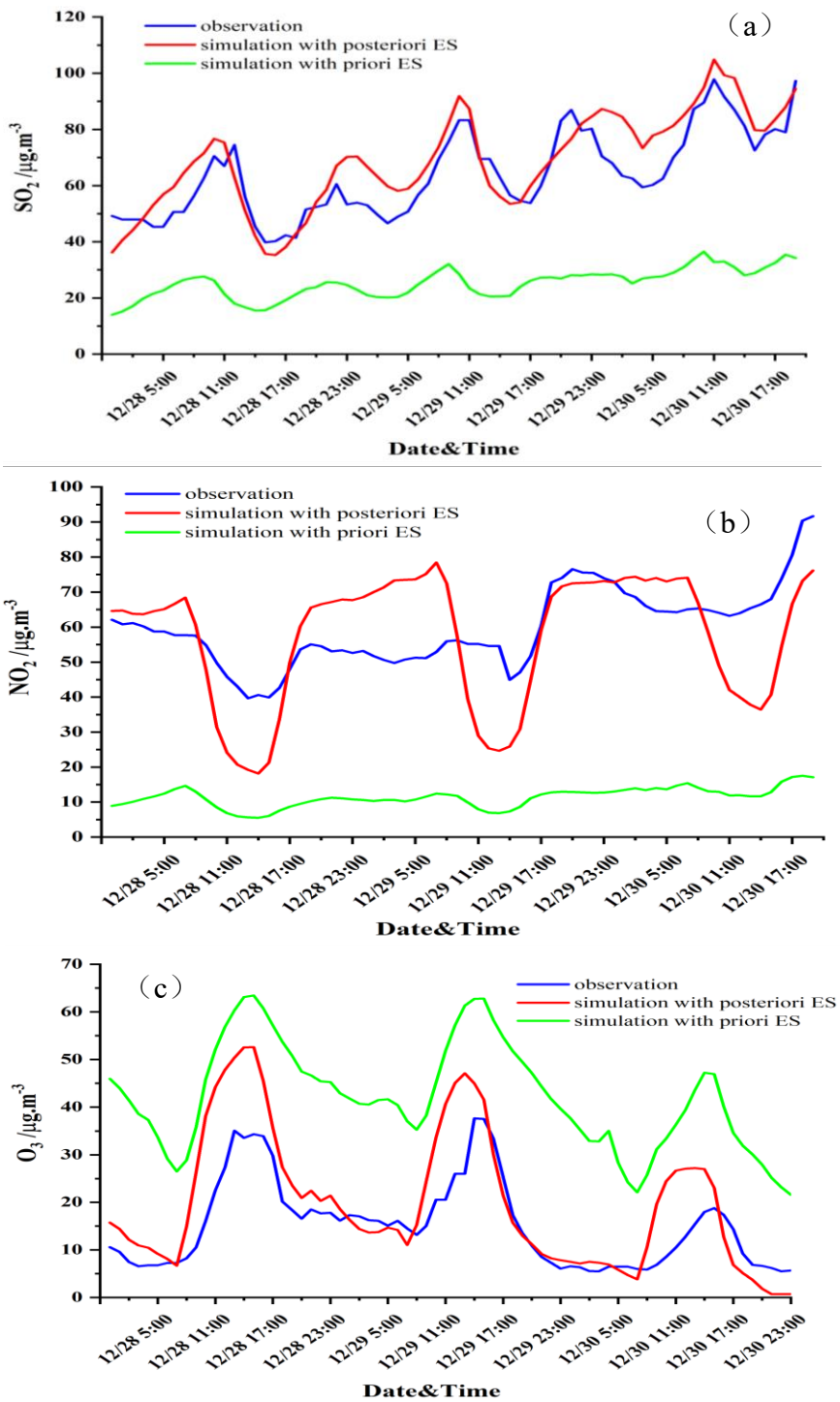

Figure 11 Time serial of regional averaged **(a)** SO_2, **(b)** NO_2, and **(c)** O_3 concentrations respectively simulated with a *priori* and a *posteriori* ES, and measurements at 45 stations in the BTH region during December 28–30, 2016.